A Secure Fingerprinting Framework for Distributed Image Classification

Guowen Xu, Xingshuo Han, Anguo Zhang and Tianwei Zhang

***Abstract*—The deep learning (DL) technology has been widely used for image classification in many scenarios, e.g., face recognition and suspect tracking. Such a highly commercialized application has given rise to intellectual property protection of its DL model. To combat that, the mainstream method is to embed a unique watermark into the target model during the training process. However, existing efforts focus on detecting copyright infringement for a given model, while rarely consider the problem of traitors tracking. Moreover, the watermark embedding process can incur privacy issues for the training data in a distributed manner. In this paper, we propose SECUREMARK-DL, a novel fingerprinting framework to address the above two problems in a distributed learning environment. It embeds a unique fingerprint into the target model for each customer, which can be extracted and verified from any suspicious model once a dispute arises. In addition, it adopts a new *privacy partitioning* technique in the training process to protect the training data privacy. Extensive experiments demonstrate the robustness of SECUREMARK-DL against various attacks, and its high classification accuracy ($> 95\%$) even if a long-bit (304-bit) fingerprint is embedded into an input image.**

***Index Terms*—Image Classification, Privacy Protection, Ownership Verification, Deep Learning.**

I. INTRODUCTION

Deep learning (DL) has become one of the most popular and powerful approaches for large-scale and complex image classification tasks, e.g., face recognition, target recognition and suspect tracking [1]–[3]. This technology has become a representative of commercialization for artificial intelligence. First, many cloud providers offer Machine Learning as a Service (MLaaS) to facilitate the deployment of DL models, e.g., Amazon Rekognition [4], Microsoft Azure Computer Vision [5], Google Cloud Vision AI [6]. Second, model vendors train customized vision models, and sell them to potential customers for profit [7]. To produce high-quality models, the vendors usually need to collect large amounts of training data from multiple data owners.

However, the aforementioned business solution still raises a wide range of concerns. The first one is the *privacy* issue. The training data from the data owners can contain very sensitive information (e.g., personal medical records, financial report, social relationships). Exposing those private data to untrusted model vendors or service providers can cause severe privacy threats. To protect the data privacy in model training, existing approaches are mostly evolved from two underlying techniques: *cryptographic primitive-based solutions* [8], [9] and *differential privacy* [10]–[12]. The former provides perfect semantic security but inevitably incurs huge computational or communication burdens, which are not suitable for training systems with limited computing and storage capabilities (refer to Section VII for more details). Compared with cryptographic protocols, differential privacy-based solutions [11], [12] are superior in performance. Unfortunately, recent research [13] shows that current deep learning frameworks based on differential privacy rarely provide acceptable practicality-privacy trade-offs for complex classification tasks. More seriously, *Hitaj et al.* [14] demonstrates that the privacy of a learning system can be fundamentally broken even if the parameters are protected by differential privacy.

The second concern is *copyright protection*. It is recognized that training a production model from scratch requires substantial hardware and labor costs for the model vendor. As a result, a commercial model is considered as precious intellectual property that needs to be properly protected. A rogue customer may purposefully use the purchased DL model to do despicable things, e.g., selling it for profit in the black market. The watermarking technology has been intensively studied to alleviate the above piracy problem. For example, by exploiting the inexplicability of deep neural networks, *Adi et al.* [15] take the backdoors of the DNNs as the watermark and embed them into the target model. These backdoors can be extracted subsequently to verify the legality of the copyright of a given model. *Rouhani et al.* [16] propose that unique secrets be embedded in the model's probability density function. Other works use a variety of strategies to achieve similar goals, including adversarial examples [17], [18], regularization parameters [19], [20], backdoors [21], [22].

However, existing works are only capable of confirming whether a target model is violated, not of monitoring traitors, i.e., rogue authorized customers who violate copyright protection regulations by spreading or manipulating the original model for profit. In reality, a model vendor usually sells a commercial model to multiple customers with the same demand. A lack of effective traitor tracking mechanisms makes it difficult for subsequent forensics when disputes arise.

In short, it is necessary to design a unified framework to realize the privacy protection of training data as well as copyright protection of the model with traitor tracking in the distributed learning setting. To the best of our knowledge, there is no previous work that can simultaneously achieve these two goals, due to the following challenges. (1) An adversary may try to erase or invalidate the watermark with a acceptable

Guowen Xu, Xingshuo Han and Tianwei Zhang are with the School of Computer Science and Engineering, Nanyang Technological University, Singapore (e-mail: guowen.xu@ntu.edu.sg; xingshuo001@e.ntu.edu.sg; tianwei.zhang@ntu.edu.sg)

Anguo Zhang is with the School of Physics and Information Engineering, Fuzhou University, China (e-mail: anguo.zhang@hotmail.com)

reduction in the performance of the original model. Such attacks including model fine-tuning and model compression have been designed and shown good attack effectiveness in practical applications. Hence, the watermark scheme should be robust enough to resist these watermark removal attacks. (2) Traitor tracking is required to embed a unique watermark (i.e., fingerprint) for each customer, rather than a uniform watermark. This distinction leads to a new attack, i.e., fingerprint collusion attack [23]. This attack means that multiple customers purchasing the same model may collude to synthesize an unlabeled model. Although this attack has been studied in the domain of multimedia [24], [25], it faces new challenges in deep learning because the countermeasures must ensure that the model is highly usable. (3) It is challenging to design a lightweight approach to protect data privacy in the training process of DNNs with fingerprints. As mentioned earlier, methods based on cryptographic primitives inevitably incur unacceptable overhead, and differential privacy has been proven to have security risks.

In this paper, we present SECUREMARK-DL, a novel and privacy-preserving deep learning framework with end-to-end ownership protection and traitor tracking[1]. We make the following two contributions. First, to protect data privacy, we propose a new *privacy partitioning* method to split a deep learning model into two parts and append a penalty function into the optimization function. This enables each data owner to obfuscate its data using an interactive adversarial deep network construction. In this way, SECUREMARK-DL significantly reduces the cost incurred for privacy protection. Second, we design a novel scheme to embed anti-collusion and unique fingerprints into the model as the proof of onwership and traitor tracking. Each fingerprint consists of two parts, i.e., Community Relationship Code (CRC) and Customer Identity Code (CIC). CRC is used to quickly screen out all potential traitors due to the social attributes between customers, while CIC is used to verify the ownership of the model. We conduct extensive experiments on three traditional datasets (MNIST, LFW and CIFAR-10). The results show that SECUREMARK-DL maintains a high classification accuracy ($> 95\%$) even if a long-bit (304-bit) fingerprint is embedded, and is also robust against various attacks, e.g., fingerprint collusion, network transformation, and private data inference.

The remainder of this paper is organized as follows. In Section II, we review some important concepts used in this paper. Then we present the technical details of SECUREMARK-DL in Section III, Section IV, and Section V. Performance evaluation and related works are discussed in Sections VI and VII. Finally, we conclude the paper in Section VIII.

II. PROBLEM STATEMENT AND DESIGN OVERVIEW

A. The Basics of Deep Learning

A typical deep neural network contains an input layer, one or more hidden layers and an output layer, where two neurons between adjacent layers are connected to each other by parameters (denoted as set Θ). As a result, the DNN model is parsed as $f_\Theta : \mathcal{X} \to \mathcal{Y}$. $\mathcal{X}$ is the space of training samples while $\mathcal{Y}$ represents all possible labels. Let the training set be $\mathcal{D} = \{(\boldsymbol{x_i}, \boldsymbol{y_i}); i = 1, 2, \cdots, V\}$, and a loss function be $l(\boldsymbol{y}, f_\Theta(\boldsymbol{x}))$ exploited to measure the difference between the prediction and the real label $\boldsymbol{y}$ (typically, $l(\boldsymbol{y}, f_\Theta(\boldsymbol{x})) = ||\boldsymbol{y} - f_\Theta(\boldsymbol{x})||_2$, where $||\cdot||_2$ is the l_2 norm of a vector), we train the model by optimizing the following objective:

$$\min_{\Theta} \frac{1}{|\mathcal{D}|} \sum_{(\boldsymbol{x},\boldsymbol{y})\in\mathcal{D}} l(\boldsymbol{y}, f_\Theta(\boldsymbol{x})). \tag{1}$$

The stochastic gradient descent (SGD) algorithm is usually used to optimize the above objective as below.

$$\Theta^{j+1} \leftarrow \Theta^j - \eta \nabla l(\mathcal{D}, \Theta^j), \tag{2}$$

where Θ^j indicates model parameters obtained from the j-th iteration, η represents the learning rate, and $\nabla l(\mathcal{D}, \Theta^j)$ is the partial derivative of Θ^j on the set $\mathcal{D}$.

B. Threat Model

We consider a scenario, where a model vendor trains an image classification model, and sells it to different customers. The training data are collected from multiple data owners. The model vendor sets up a training framework using a cloud service. Fig. 1 illustrates our system model.

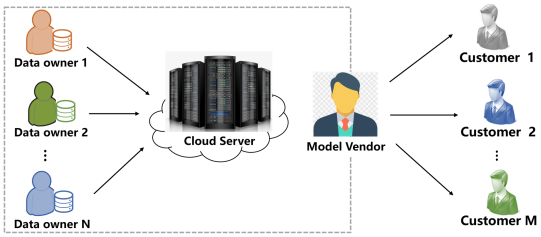

Fig. 1: System model in our consideration

Consistent with most existing works [9], [26], [27], data owners and the cloud server are considered honest but curious, which means that they honestly interact with each other in training the DNN model but may try to deduce sensitive information of other participants based on the knowledge they obtain. Customers are malicious: they can abuse the DNN model purchased from the model vendor; they try to delete or invalidate the possible fingerprints embedded in the model to avoid traitor tracking. We allow the collusion of multiple customers to attack our fingerprinting mechanism, with the following strategies:

(1) *Model Fine-tuning*. This is used to retrain a well-trained model so that it can be applied to other applications with comparable functions. This is very efficient because training a DL model from scratch requires substantial hardware and labor costs. However, an adversary can seize this feature to weaken the stability of the fingerprint. Retraining the model makes it difficult to extract the fingerprint embedded in the model parameters.

[1]This paper is an extension of our previous work [3]

(2) *Model Compression*. This is a standard optimization technique by cropping the capacity of the original model. It can reduce the computational overhead of the prediction process and has only a slight performance degradation compared to the original model. An adversary can abuse this optimization to prune the hidden layers and possibly erase the fingerprints in the model.
(3) *Fingerprint Collusion*. Multiple customers who have purchased the same model can collude to erase or invalidate the fingerprint embedded in the model. We focus on the average fingerprint collusion attack [23], where conspirators take the average of the parameters of the models they hold as the parameters of the newly generated model.

C. Design Goals

We formulate the following goals for a qualified privacy-preserving fingerprinting framework.

(1) *Utility*. We need to ensure that the DNN model from the framework has negligible accuracy loss compared to the original model.
(2) *Privacy*. The framework should guarantee data privacy of all data owners, i.e., any data owner cannot derive the sensitive data of other owners, and the cloud server cannot recover the data from any owner from the training process.
(3) *Fingerprint Security*. First, it requires the embedded fingerprint to be unique, which facilitates quick detection of suspicious customers. Second, the embedded fingerprint should perform well in terms of reducing false positives and false negatives, which means that the model vendor has a high probability of detecting a traitor, and a low probability of accusing innocent customers. Third, the embedded fingerprint should be robust against various attacks such as fingerprint collusion, model compression, and model fine-tuning.
(4) *Scalability*. The framework should be suitable for model release and ownership verification for large-scale customer groups. It should have the ability of embedding long-bit fingerprints, where the model accuracy is statistically independent of the fingerprint size. Moreover, it is also required to track all traitors efficiently, even the target model is released to a large number of customers.

D. Framework Overview

Fig. 2 shows the overview of our SECUREMARK-DL framework. We consider a system with N *data owners*, a *cloud server* and M *customers*. We use Θ to denote the DNN model demanded by the customers. SECUREMARK-DL adopts two techniques to protect the privacy and copyright of Θ.

First, we leverage the model splitting technique to preserve the training data of each owner. Specifically, the model Θ is split into two parts: Θ_l is the local network and Θ_r is the remote network. Θ_l is distributed to all the data owners while Θ_r is kept on the cloud server. Then the data owners and server collaboratively train the model and update their own networks. In this way, the data owners do not need to share their private data with others. To further prevent the information leakage from the intermediate parameters, each data owner exploits an adversarial DNN to perturb the parameters before uploading them to the cloud server. We give the technical details in Section III.

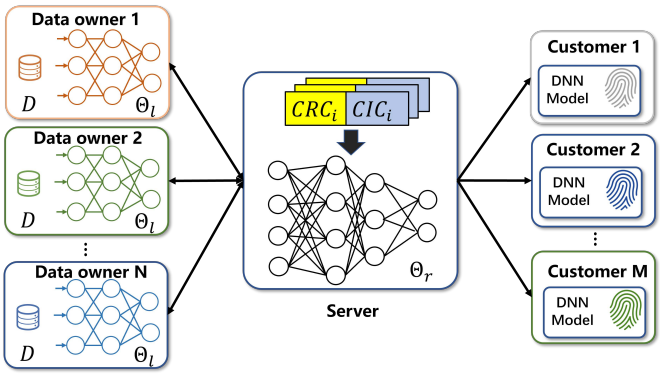

Fig. 2: Overview of SECUREMARK-DL

Second, for each customer i, SECUREMARK-DL selects an independent fingerprint F_i for ownership protection, and enforces the cloud server to embed it to Θ_r during the above training process. Subsequently, the model vendor can extract the fingerprint from the suspicious model and check the ownership of the model or track traitors. Specifically, F_i contains two parts, i.e., F_i=(p_i|| u_i). The first part p_i is Community Relation Code, which is used to quickly track all potential traitors. It is built using the Neighborhood Preserving Hashing (NPH) primitive [28]. On the Hamming space, NPH can be used to map high-dimensional objects into low-dimensional binary vectors (also known as hash codes). Furthermore, NPH preserves object neighborhood structure, i.e., codes of similar objects will have a small Hamming distance. The second part u_i is Customer Identity Code, which is used to verify the model ownership. It is built using the balanced incomplete block design (BIBD) [29], which ensures that the synthesized code of any K or smaller customer identity codes remains unique. This can accurately find fingerprint collusion among K or fewer customers. More details about fingerprint generation, extraction and verification will be presented in Section IV.

III. PRIVACY PARTITIONING FOR DISTRIBUTED LEARNING

Our goal is to protect the training data of each data owner from being leaked to other participants. One possible solution is federated learning, where each data owner trains a local model, and only uploads the gradients to the cloud server for aggregation. However, the data owners may not have enough computing power to train an entire model. Besides, past works have demonstrated that the gradients can also leak sensitive information about the training data [14]. Hence, we decide to adopt a more sophisticated solution in SECUREMARK-DL: privacy partitioning [30]. The basic idea is to split the model into two parts, asking the data owners and server coordinately train their individual parts to produce the final model. However, the solution in [30] only allows two-party model splitting. We enhance it to support the collaboration between multiple data owners and a server.

Concretely, given a DNN Θ, we split it into two parts: $\Theta = \{\Theta_l, \Theta_r\}$. Fig. 3 depicts the specific structure of the bipartite topology, where Θ_l is assigned to each data owner, and the completed Θ is maintained in the server. The hidden state $\mathcal{H} = (h_1, h_2, \cdots h_S)$ is the output of the last layer L_i in Θ_l, and the input of the first layer L_{i+1} in Θ_r.

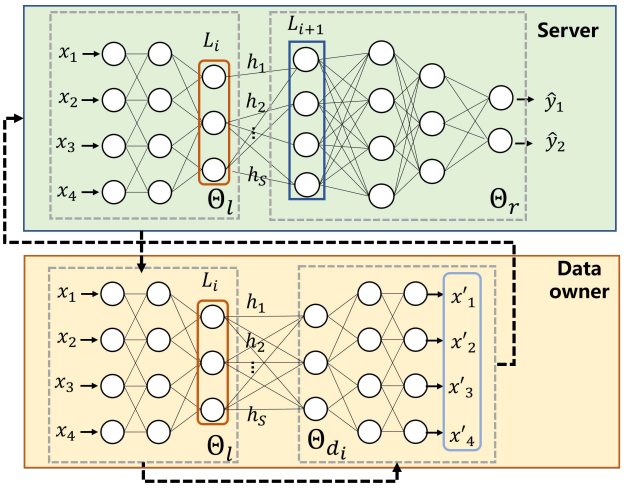

Fig. 3: Model training with privacy partitioning

Assume each data owner holds a local dataset $\mathcal{D}_i$. Then it first derives the hidden state $\mathcal{H} = (h_1, h_2, \cdots h_S)$ by running Θ_l with $\mathcal{D}_i$. To prevent the adversary from reconstructing the training data from the hidden state, we introduce an interactive adversarial DNN Θ_{d_i} for each data owner, whose goal is to obfuscate $\mathcal{H}$ so that it is not feasible for the adversary to derive the original data from the hidden state. It simulates the adversary by attempting to recover the training data from the output of Θ_l. Hence, the function of Θ_{d_i} can be described as $f_{\Theta_{d_i}} : \mathcal{H} \rightarrow \mathcal{X}$. For each data owner, the goal of Θ_{d_i} is formulated as:

$$\min_{\Theta_{d_i}} \frac{1}{|\mathcal{D}_i|} \sum_{(\boldsymbol{x},\boldsymbol{y})\in\mathcal{D}_i} -d(\boldsymbol{x}, f_{\Theta_{d_i}}(f_{\Theta_l}(\boldsymbol{x}))), \tag{3}$$

where $d(\cdot,\cdot)$ is the privacy distance metric to describe the similarity between the recovered input from Θ_{d_i} and the original input.

With the adversarial DNN Θ_{d_i}, each data owner can produce obfuscated training samples $\mathcal{D}'_i = \{f_{\Theta_{d_i}}(f_{\Theta_l}(\boldsymbol{x})), y\}$ which are different from $\mathcal{D}_i$. The server collects those obfuscated samples from all the data owners as $\mathcal{D}' = \cup_{i=1}^{i=N}\mathcal{D}'_i$, and uses them to train the complete model $\Theta = \{\Theta_l, \Theta_r\}$. This can be done via the traditional SGD method with the objective in Eqn. 1. Then the server sends the local model Θ_l back to each data owner.

It is worth noting that each Θ_{d_i} is trained concurrently with the original network Θ, as shown in Algorithm 1. Each data owner updates Θ_{d_i} based on Θ_l. With the new Θ_{d_i}, the data owner produces new data samples for the server to update Θ_l and Θ_r. Then Θ_r is sent back to the data owner for the network update at the next round. The cooperation between the data owners and server ensures the final model Θ can achieve satisfactory performance. Meanwhile, the data owners do not need to share their data with the server.

IV. Fingerprint Generation and Embedding

We describe the details of generating a unique fingerprint for each customer. Typically, the fingerprint is generated by the server and is usually embedded in the remote network Θ_r, as this helps to protect its confidentiality. Considering the large-scale nature of customers in the internet environment, we introduce social networking between customers for fingerprint generation. In social networks, recent work [31] has pointed out that people in similar communities are more likely to band together to accomplish similar goals, while people in different communities have a very low probability of doing so. Based on this, we create a two-tier fingerprint structure in which each customer's fingerprint F_i contains two parts, F_i=(p_i|| u_i). p_i indicates the community relationship code denoted the social network structure of the customer i. Customers in similar communities will be assigned community relationship codes that are similar, whereas unrelated customers will be assigned community codes that are very different. This attribute is used to quickly identify suspicious customer groups. u_i is a unique customer identity code, where BIBD [29] is exploited to generate the anti-collusion identity code for each customer. Such customer identity codes ensure that the synthesised code of any K or smaller customer identity code remains unique.

Remark: Our designed fingerprint structure is functionally compatible with the representative works of group-oriented fingerprint (GOF) [32] in the multimedia field. GOF introduces the group idea and customers by the geographical relationship, which significantly improves the performance of anti-collusion if the colluders are from the same group. However, GOF is not applicable to our scenario. Firstly, constructing orthogonal codes independently for each geographic location-based group can only represent the social network unilaterally, and the efficiency of coding decreases significantly as the number of groups increases. On the other hand, the group in GOF is fixed, which is also not suitable for dynamic social networks. In the following description, we first introduce how to construct a community code and customer identity code for each customer, respectively. Then we describe the implementation of embedding fingerprints with privacy-preserving training.

A. Generating Community Relationship Code

Since the social relationship between customers is usually established by the geographical distance, activity range, blood relationship, and many unknown factors, this leads to the high-dimensional customer relationship in social networks. If we directly employ these high-dimensional vectors to represent customer relationships and integrate them in the DNN parameters, the fingerprint's dimensionality will definitely reduce the accuracy of the original model. To address this problem, the primitive Neighborhood Preserving Hashing (NPH) [28] is introduced to break this bottleneck. To be precise, high-dimensional objects can be mapped to low-dimensional binary vectors on the Hamming space through NPH. Furthermore,

codes of similar objects will have a small Hamming distance. Motivated by this, we propose an NPH-based community code generation method as follows.

Assuming that the social link between consumers is represented by an adjacency matrix. We create an adjacent matrix as shown below.

$$\Gamma_{ij} = \begin{cases} 1 : \text{if } \mathcal{B}_i \in \mathcal{C}(\mathcal{B}_j) \text{ or } \mathcal{B}_j \in \mathcal{C}(\mathcal{B}_i) \\ 0 : \text{otherwise} \end{cases} \tag{4}$$

where $\mathcal{C}(\mathcal{B}_j)$ refers to the set of customers contacting with thethe j-th customer $\mathcal{B}_j$, with $i, j = 1, \cdots M$. It should be noted that we do not make any assumptions about the customer's social network. This means that the original social network can be built from the server's long-standing experience or the public information. Based on this, we explain the technical details of NPH, which consists of two parts, i.e., Locally Linear Embedding(LLE) [33] and Non-negative Matrix Factorization (NMF) [34].

Specifically, we can use NMF to approximately decompose a high-dimensional matrix into a product of two low-dimensional matrices. For any non-negative matrix $G = [g_1, g_2, \cdots g_M] \in \mathtt{R}^{E\times M}$, it is feasible to construct two matrices, denoted as $B = [b_1, b_2, \cdots, b_T] \in \mathtt{R}^{E\times T}$ and $F = [F_1, F_2, \cdots, F_M] \in \mathtt{R}^{T\times M}$, where the the product of the two matrices is approximately matrix B. More concretely, we have

$$\begin{aligned} &\min_{M,F} ||G - BF||_F^2 \\ &\mathsf{s.t.} \quad B \geq 0,\ F \geq 0 \end{aligned} \tag{5}$$

where $||\cdot||_F$ is the Frobenius norm of a matrix, and g_i is the properties of customer i. F_i is the low-dimensional representation of g_i, and B indicates a dictionary matrix.

While the semantic information is preserved in the process of converting g_i to F_i, the neighbor structure between different g_i may be lost. This means that customers from the same community may be completely different in coding. LLE [33] is exploited to break this dilemma. LLE is founded on the idea that if an object can be reconstructed from its neighbors in the original high-dimensional space, it can likewise be reconstructed from the low-dimensional subspace's neighbors. LLE achieves the stated goal by minimizing the reconstruction error as shown below, given a g_i.

$$\begin{aligned} &\min_{\omega} \sum_{i=1}^{i=M} |g_i - \sum_{g_j \in \mathcal{N}(g_i)} \omega_{ij} g_j|_2^2 \\ &\mathsf{s.t.} \quad \sum_{g_j \in \mathcal{N}(g_i)} \omega_{ij} = 1 \end{aligned} \tag{6}$$

where the k-nearest neighbors of g_i are represent as $\mathcal{N}(g_i)$. Then, let F_i be the representation of g_i in a low-dimensional space, LLE further minimizes the following function to maintain the neighbor relationship of g_i.

$$\begin{aligned} &\min_{F} \sum_{i=1}^{i=M} |F_i - \sum_{i} \omega_{ij} F_j|_2^2 \\ &\mathsf{s.t.} \quad F \geq 0 \end{aligned} \tag{7}$$

This ensures that the community relationship codes between g_i and g_j are very close if they are from the same or similar communities.

Combining the properties of NMF and LLE, we describe the details of generating the community relationship code. Specifically, we first rewrite Eqn.(5) as follows.

$$\begin{aligned} &\min_{B,F} \sum_{i=1}^{i=M} |g_i - BF_i|^2 \\ &\mathsf{s.t.} \quad B \geq 0,\ F \geq 0 \end{aligned} \tag{8}$$

Then, we modify Eqn.(8) as follows.

$$\begin{aligned} &\min_{B,F} \sum_{i=1}^{i=M} |g_i - \sum_{j} \omega_{ij} BF_i|^2 \\ &\mathsf{s.t.} \quad B \geq 0,\ F \geq 0 \end{aligned} \tag{9}$$

where $g_j \in \mathcal{N}(g_i)$. Then, we have

$$\begin{aligned} &\min_{B,F} ||G - BFW^T||_F^2 \\ &\mathsf{s.t.} \quad B \geq 0,\ F \geq 0 \end{aligned} \tag{10}$$

At this point, we can obtain vector F_i by solving Eqn.(10), which is used to represent g_i.

1) Solving Algorithm: Eqn.(10) is not a convex function in the domain of B and F, according to the optimization theory. As a result, determining the global optimal value is impossible. Eqn.(10), on the other hand, is alternatively convex on B and F. To find local minima, many numerical optimization methods such as multiplicative update [35], gradient descent [**?**], and projection gradient [37] are used. We exploit the projection gradient method to solve the above objective function due to its fast convergence speed. Let $\mathcal{O} = ||G - FFW^T||_F^2$, we have

$$\begin{aligned} \mathcal{O} &= tr[(G - BFW^T)(G - BFW^T)^T], \\ &= tr(GG^T) - 2tr(GWF^TB^T) + tr(BFW^TWF^T), \end{aligned} \tag{11}$$

where we use $tr(\cdot)$ to indicate the matrix trace. With the properties of $tr(AB) = tr(BA)$ and $tr(A) = tr(A^T)$, we can compute the partial derivatives for B and F as follows.

$$\begin{aligned} \frac{\partial \mathcal{O}}{\partial B} &= 2BFW^TWF^T - 2GWF^T, \\ \frac{\partial \mathcal{O}}{\partial F} &= 2B^TBFW^TW - 2B^TGW. \end{aligned} \tag{12}$$

The objective function will then be treated as two independent sub-problems, with one variable updated while the other variable's value remains constant. Specifically, for any i, j, with $B_{ij}^1 \geq 0$, $F_{ij}^1 \geq 0$, the two subproblems are as follows.

$$\widetilde{f}(F^{k+1}) = \arg\min_{F \geq 0} f(B^k, F^k), \tag{13}$$

$$\widetilde{f}(B^{k+1}) = \arg\min_{B \geq 0} f(B^k, F^{k+1}). \tag{14}$$

We take Eqn.(10) as an example to describe the details of solving the above problems. Specifically, Eqn.(10) is first rewritten as below.

$$\begin{aligned} &\min_{F} \widetilde{f}(F) = ||G - BFW^T||_F^2 \\ &\mathsf{s.t.} \quad F_{i,j} \geq 0, \forall i, j \end{aligned} \tag{15}$$

Since F, W are given matrices and B is initialized by a random non-negative matrix, the update of F_i^k to F_i^{k+1} is shown as follows.

$$F_i^{k+1} = F[F_i^k - \alpha^k \nabla \widetilde{f}(F_i^k)], \tag{16}$$

Then we have

$$F_{ij} = \begin{cases} 0 : F_{ij} \leq 0 \\ F_{ij} : \text{otherwise} \end{cases} \tag{17}$$

Therefore, for any α, $F_i^{k+1} = F[F_i^k - \alpha^k \nabla \widetilde{f}(F_i^k)]$, we have

$$\widetilde{f}(F_i^{k+1}) - \widetilde{f}(F_i^k) = \sigma \nabla \widetilde{f}(F_i^k)^T (F_i^{k+1} - F_i^k), \tag{18}$$

where σ represents a small positive constant. Based o the Taylor approximation for $\widetilde{f}$ at F_i^k up to second order, i.e.,

$$\widetilde{f}(F_i^{k+1}) \approx \widetilde{f}(F_i^k) + \nabla \widetilde{f}(p_i^k)^T \upsilon + \frac{1}{2} \upsilon^T \nabla^2 \widetilde{f}(F_i^k) \upsilon, \tag{19}$$

where $\nabla^2 \widetilde{f}(\cdot)$ indicates the Hessian matrix of $\widetilde{f}(F)$, $\upsilon = (F_i^k)^T (F_i^{k+1} - F_i^k)$, Eqn.(19) is expressed as

$$(1 - \sigma) \nabla \widetilde{f}(F_i^k)^T \upsilon + \frac{1}{2} \upsilon^T \nabla^2 \widetilde{f}(F_i^k) \upsilon \leq 0. \tag{20}$$

Then, once the optimal α is obtained, Eqn. (16) is iteratively updated to find a stable F. Later, Eqn. (15) is rewritten with a similar method to find the optimal G as follows.

$$\begin{aligned} &\min_B \widetilde{f}(B) = ||G^T - WF^T B^T||_F^2 \\ &\text{s.t.} \quad B_{i,j} \geq 0, \forall i, j \end{aligned} \tag{21}$$

2) Kernel Trick: We know that when G is given, the above problems are easily solved. However, it is difficult to obtain the attributes of each customer ((i.e., $G = [g_1, g_2, \cdots g_M]$)) in real scenarios. To solve the above problem, we introduced the kernel skill trick [38]. Assume there is a high-dimensional matrix G, which is not used in practice, and a map that maps Euclidean space $\mathtt{R}^M$ to the Hilbert space $\mathtt{Z}$, i.e., $\phi : \mathtt{R}^M \rightarrow \mathtt{Z}$. Let $\phi(G)$ be the matrix in the Hilbert space, where $\phi(G) = [\phi(g_1), \phi(g_2), \cdots, \phi(g_M)]$. Then, Eqn.(10) can be modified as follows.

$$\begin{aligned} &\mathcal{O} = \min_{B,F} ||\phi(G) - BFW^T||_F^2 \\ &\text{s.t.} \quad B \geq 0,\ F \geq 0 \end{aligned} \tag{22}$$

Eqn.(23) is further modified as follows

$$\begin{aligned} \mathcal{O} &= tr[(\phi(G) - BFW^T)(\phi(G) - BFW^T)^T], \\ &= tr(Q) - 2tr(\phi(G) W F^T B^T) + tr(BFW^T W F^T). \end{aligned} \tag{23}$$

Then, we define the dot product over the Hilbert space as below.

$$Q(g_i, g_j) = (\phi(g_i) \cdot \phi(g_j)) = \phi(g_i)^T \phi(g_j).$$

Since B is a linear combination of $\phi(g_1)$, $\phi(g_2)$, $\cdots$, $\phi(g_M)$, we can find a coefficient matrix C such that $B = \phi(G)C^T$. We replace B with $\phi(G)C^T$ in Eqn.(24), and obtain the following objective function:

$$\begin{aligned} &\mathcal{O} = \arg\min_{C,F} (tr(Q) - 2tr(QC^T FW) + tr(WF^T CQC^T FW^T)) \\ &\text{s.t.} \quad C \geq 0,\ F \geq 0 \end{aligned} \tag{24}$$

Eqn.(24) shows that B is not required to solve the above objective function. In fact, the kernel matrix Q, which is built on the matrix B, represents the similarity of each data set. As a result, the kernel function's purpose is to generate a similarity matrix with black-box access to G. Because the adjacency matrix γ (as shown in Eqn.5) is also used to express similarity, we can use it directly to replace the kernel function. In practice, the server may struggle to obtain G for each customer, but we can use the adjacency matrix to solve the above problem and finally obtain the community relationship code for each customer.

B. Generating Customer Identity Code

Obviously, community relationship codes cannot uniquely represent each customer due to their collision in coding. To address this problem, the technology of BIBD [29] is adopted to generate additional unique customer identity code for each customer. Moreover, such a customer identity code can ensure that the combination of any K or fewer customers on the code is still distinguishable. In short, we use a pair $(\Psi, \mathcal{A})$ to define the (g, k, γ)-BIBD, where Ψ is a set containing g-dimensional elements, and $\mathcal{A}$ indicates the collection of k-element subsets (blocks). It ensures that each pair of Ψ elements appears together exactly γ times in the subsets [23]. The (g, k, γ)-BIBD has a total of $t = \gamma(g^2 - g)/(k^2 - k)$ blocks (k is the block sizes) which can be represented by its corresponding incidence matrix $\mathtt{C}_{g \times t}$. Specifically, elements in $\mathtt{C}_{g \times t}$ have the following connections:

$$c_{ij} = \begin{cases} 1 : \text{if } i^{th} \ value \ occurs \ in \ j^{th} \ block \\ 0 : \text{otherwise} \end{cases} \tag{25}$$

If we set $\gamma = 1$, the $(g, k, 1)$-BIBD code is $(k-1)$-resilient. Given $\mathtt{C}_{g \times M}$ and let $\mathcal{F}_{g \times g} = (\mathtt{f}_1, \mathtt{f}_2, \cdots, \mathtt{f}_g)$ be an orthogonal matrix, we can first compute a coefficient matrix $\mathcal{E}_{g \times M}$ with $e_{ij} = 2c_{ij} - 1$. Then, the customer identity code u_j for each customer j is computed as below.

$$u_j = \sum_{i=1}^{i=g} e_{ij} \mathtt{f}_j. \tag{26}$$

C. Embedding Fingerprint

We have described the details of generating a fingerprint F_j=(p_j|| u_j) for each customer j, where p_j is the community relationship code p_j, and u_j is the customer identify code. The technical details of embedding F_j into the parameters of Θ are presented in this section. In brief, F_j is embedded into the parameters of the remote network Θ_r by adding an additional regularization loss during training. This is mainly inspired by the high dimensionality of DNNs, that is, there are a large number of redundant parameters in the DNN model. This redundancy is helpful for embedding fingerprints as an auxiliary task in training without significantly impairing the classification accuracy of the original model. In addition, the inexplicability of the model makes the embedded fingerprints integrated as a component of the parameters, so that the adversary cannot accurately locate where the fingerprint is embedded in the model. This makes it difficult for adversaries to remove fingerprints without significantly impairing the

performance of the marking model. To achieve this, some hidden layers (usually convolutional layers) in Θ_r are first selected to prepare for embedding fingerprints, where we use the symbol $\theta^{sub} \in \Theta_r$ to denote the parameters belonging to the selected layers. Then, a new term $\mu MSE(F_j - \mathbf{X}\Theta_r^{sub})$ is added into the original objective function (shown in Eqn.(3)). As a result, the server is required to embed F_j with training the following objective function.

$$\min_{\Theta} \frac{1}{|\mathcal{D}|} \sum_{(\boldsymbol{x},\boldsymbol{y})\in\mathcal{D}} l(\boldsymbol{y}, f_\Theta(\boldsymbol{x})) + \mu MSE(F_j - \mathbf{X}\Theta_r^{sub}), \tag{27}$$

where MSE is the mean square error function, μ indicates the embedding weight, and $\mathbf{X}$ is the secret random projection matrix. Θ_r^{sub} represents flattened averaged parameters of θ^{sub} for embedding F_j.

In summary, F_j is embedded into Θ_r. We know that θ^{sub} are 3D tensors, i.e., $\theta^{sub} \in \mathtt{R}^{S\times\delta\times\eta}$, where S is the length of Θ_r, δ is the kernel size and η is used to denote the number of channels in Θ_r. Hence, to embed the fingerprint, the average of θ^{sub} over all channels is first computed, and then we stretch it into a vector $\Theta_r^{sub} \in \mathtt{R}^{\beta}$, where $\beta = S \times \delta$. It has been demonstrated that changing the order of the filtering channels has no effect on the output of the neural network, even though the parameters in the subsequent layers are rearranged accordingly. Therefore, We take as an additional term $\mu MSE(F_j - \mathbf{X}\Theta_r^{sub})$ added into the objective function, whose goal is to minimize the difference between F_j and $\mathbf{X}\Theta_r^{sub}$ during training. The implementation details of our SECUREMARK-DL is shown in **Algorithm 1**.

Algorithm 1: Implementation of SECUREMARK-DL

Input: Training set $\mathcal{D} = \cup_{i=1}^{i=N}\mathcal{D}_i$, customer j's fingerprint F_j.
Output: Trained model f_Θ embedded fingerprint F_i, where $\Theta = \{\Theta_l, \Theta_r\}$.
Initialize: Parameters of Θ and defender Θ_{d_i}, $i \in [1, N]$.
for $t \le \max_{it}$ **do**
  for *Each data owner* i **do**
    1. Randomly select a subset $\mathcal{D}_i^{sub} \in \mathcal{D}_i$;
    2. Update the parameters of Θ_{d_i} via gradient descent as follows:

$$\nabla_{\Theta_{d_i}} \frac{1}{|\mathcal{D}_i^{sub}|} \sum_{(\boldsymbol{x},\boldsymbol{y})\in\mathcal{D}_i^{sub}} -d(\boldsymbol{x}, f_{\Theta_{d_i}}(f_{\Theta_l}(\boldsymbol{x})))$$

    3. Take $f_{\Theta_{d_i}}(f_{\Theta_l}(\boldsymbol{x}))$ as input of Θ_l and upload the output to the server. Please note that here we use artificial data generated by Θ_{d_i} in place of real data for training.
  end
  for *the server* **do**
    1. Update the parameters of $\Theta = \{\Theta_l, \Theta_r\}$ via SGD as follows:

$$\nabla_\Theta \frac{1}{|\mathcal{D}^{sub}|} \sum_{(\boldsymbol{x},\boldsymbol{y})\in\mathcal{D}^{sub}} l(\boldsymbol{y}, f_\Theta(\boldsymbol{x})) + \mu MSE(F_j - \mathbf{X}\Theta_r^{sub})$$

    2. Return the parameters of Θ_l to all data owners.
  end
end

Remark: As mentioned in Section III, each defender network Θ_{d_i} is trained concurrently with the original network Θ. Once the parameters of Θ_l is returned to all data owners, every data owner can adaptively train the defender network Θ_{d_i} based on the feedback of Θ_l. Although existing work [39] has stated that such adversarial training methods may help adversaries (i.e., the cloud server) to perform data reverse-engineering attacks, as explained before, the cloud server is considered honest but curious (that is, passive) in our scenario, which means that it honestly interacts with each other in the training process. As a result, this type of attack is beyond the scope of this paper.

V. FINGERPRINT EXTRACTION AND VERIFICATION

In order to verify the ownership of the model, the server needs to extract fingerprints from the suspicious model and obtain evidence to discover possible infringements. To achieve this, we first review the principles of fingerprint embedding in SECUREMARK-DL, i.e., minimizing the difference between F_j and $\mathbf{X}\Theta_r^{sub}$ during training. Therefore, to get the fingerprint from a suspicious model, the server only needs to obtain the parameter θ^{sub} of the target layer, and calculate the flattened and averaged version Θ_r^{sub}. Then, the fingerprint F_j can be recovered by computing $F_j = \mathbf{X}\Theta_r^{sub}$. To quickly find traitors, Then, all customers in the selected community will be regarded as potential traitors. Finally, we use the attributes of the customer identity code to pinpoint the colluding customers.

We have mentioned that the technology of BIBD [29] is adopted to generate the customer identity code for each customer. It possesses the attribute that combination of any K or fewer customers on the code is still distinguishable. To demonstrate that, we use a $(7, 3, 1)$-BIBD codebook to illustrate the workflow of collusion detection utilizing the customer identity code. Specifically, given the incidence matrix $\mathtt{C}$ (shown in Eqn.(28)), the identity code of each customer is shown in Eqn.(29).

$$\mathtt{C} = \begin{bmatrix} 0 & 0 & 0 & 1 & 1 & 1 & 1 \\ 0 & 1 & 1 & 1 & 0 & 1 & 1 \\ 1 & 0 & 1 & 0 & 1 & 0 & 1 \\ 0 & 1 & 1 & 1 & 1 & 0 & 0 \\ 1 & 1 & 0 & 0 & 1 & 1 & 0 \\ 1 & 0 & 1 & 1 & 0 & 1 & 0 \\ 1 & 1 & 0 & 1 & 0 & 0 & 1 \end{bmatrix} \tag{28}$$

$$\begin{cases} u_1 = -\mathtt{f}_1 - \mathtt{f}_2 + \mathtt{f}_3 - \mathtt{f}_4 + \mathtt{f}_5 + \mathtt{f}_6 + \mathtt{f}_7 \\ \cdots \\ u_6 = \mathtt{f}_1 + \mathtt{f}_2 - \mathtt{f}_3 - \mathtt{f}_4 + \mathtt{f}_5 + \mathtt{f}_6 - \mathtt{f}_7 \\ u_7 = \mathtt{f}_1 + \mathtt{f}_2 + \mathtt{f}_3 - \mathtt{f}_4 - \mathtt{f}_5 - \mathtt{f}_6 + \mathtt{f}_7 \end{cases} \tag{29}$$

where $\mathcal{F} = (\mathtt{f}_1, \mathtt{f}_2, \cdots, \mathtt{f}_g)$ is an orthogonal matrix selected by the server. For customer 1, its coefficient vector $\mathbf{e_1}$ can be computed as

$$\mathbf{e_1} = u_1^T[\mathtt{f}_1, \cdots, \mathtt{f}_7] = [-1, -1, 1, -1, 1, 1, 1]$$

Then $\mathbf{c_1}$ can be recovered by the inverse linear mapping $c_{ij} = \frac{1}{2}(e_{ij} + 1)$. This consistency ensures that the anti-collusion (ACC) identity code can be used to identify individual customers.

Colluder detection. Now we introduce how to use the customer identity code to resist the average collusion attack of multiple customers. Suppose the conspirators take the average of the parameters of the model they hold as the parameters of the newly generated model, where we use Θ_{avg}^{sub} as the

changed parameters of targeted layers used to embed the fingerprint. In order to detect the collusion, the server first calculates $F^{avg} = \mathbf{X}\Theta^{sub}_{avg}$, and then extracts the customer identity code segment u^{avg}. As a result, the coefficient vector $\mathbf{e}^{avg}$ can be computed as $\mathbf{e}^{avg} = (u^{avg})^T\mathcal{F}$. Assuming that $\mathbf{e}^{avg} = (e_1^{avg}, e_2^{avg}, \cdots, e_g^{avg})$, the server calculates c_i^{avg} with a threshold τ as follows.

$$c_i^{avg} = \begin{cases} 1 : \text{if } e_i^{avg} > \tau \\ 0 : \text{otherwise} \end{cases} \tag{30}$$

where SECUREMARK-DL adopts the hard-thresholding detector [40], [41] to track colluders. Next, given the $\mathbf{c}^{avg} = (c_1^{avg}, c_2^{avg}, \cdots, c_g^{avg})$, the problem of finding colluders is equivalent to solving the problem of finding the subsets of columns from incidence matrix $\mathtt{C}$, where the logic-AND composition on these columns are exactly equal to $\mathbf{c}^{avg}$. For example, assume customers 6 and 7 are the colluders who generate the average customer identity code as follows.

$$u^{avg} = \frac{1}{2}(u_6 + u_7) = \frac{1}{2}(2\mathtt{f}_1 + 2\mathtt{f}_2 - 2\mathtt{f}_4)$$

The server computes the coefficient vector $\mathbf{e}^{avg}$ as below.

$$\mathbf{e}^{avg} = (u^{avg})^T\mathcal{F} = [1, 1, 0, 0, 0, 0, 0]$$

As a result, based on the Eqn. (30), $\mathbf{c}^{avg}$ can be extracted as $\mathbf{c}^{avg} = [1, 1, 0, 0, 0, 0, 0]$. We can observe that the logic-AND of columns 6 and 7 in $\mathtt{C}$ is exactly equal to $\mathbf{c}^{avg}$, while operations on other columns cannot produce the same result. This instance demonstrates that the colluders can be uniquely identified by the BIBD-based customer identity code.

VI. PERFORMANCE EVALUATION

We undertake experiments to evaluate the performance of our SECUREMARK-DL. Each data owner in our experiments has a smartphone with 6GB RAM and the Android 6.0 operating system. The " Cloud " is replicated using a Lenovo server with an Intel(R) Xeon(R)E5-2620 2.10GHz CPU, 16GB RAM, 256SSD, 1TB mechanical hard disk, and Ubuntu 18.04. each customer is given an HP i7 8550u notebook with a 1.8GHz CPU, 8GB flash memory, 256GB SSD, and 500GB mechanical hard drive, as well as the 64-bit Windows 10 operating system. We first experimentally demonstrate the high privacy-preserving level of SECUREMARK-DL in Section VI-A, where we verify the performance of the proposed *Privacy Partitioning* on three different datasets, i.e., MNIST[2], LFW[3] and CIFAR-10[4]. Then, in Section VI-B, we further analyze the performance of the designed fingerprint, and demonstrates demonstrate its robustness against various attacks.

[2]http://yann.lecun.com/exdb/mnist/
[3]http://vis-www.cs.umass.edu/lfw/
[4]https://www.cs.toronto.edu/ kriz/cifar.html

A. Performance of Privacy Partitioning

In the discipline of computer vision, determining how to measure an image's privacy breach has long been a difficult subject. In very diverse application settings, different persons have quite varying privacy requirements. In general, in the field of computer vision, indistinguishable metrics are often used to evaluate the quality of pictures relative to the benchmark picture. Common metrics such as MSE (Mean Squared Error) [42], [43], SSIM (Structural Similarity Index) [44], [45], and DPD (Deep Perceptual Distance) [46], [47], are widely used to quantify the human perceptual capability over images. In our experiments, we estimate the indistinguishability between recovered images and the original images using a set of measures (given below), which will serve as a proxy for quantifying image privacy leakage.

- *MSE*. This method is used to calculate the perpixel l-2 Euclidean distance between two images, which can be used to assess image reconstruction quality. That is, the smaller the MSE value between the two images, the higher the similarity between the two. However, relying solely on MSE is not sufficient because it assumes that pixels are independent of each other. One can blur an image to change the l-2 Euclidean distance slightly but cause a large change in perception.
- *SSIM*. This method is computed to capture the structural information between two images, which improves the performance of MSE because of the assumption that the elements are not mutually independent [44], [45]. SSIM is ranged from $[-1, 1]$, where SSIM $= 1$ means that the given two images are identical.
- *DPD*. Recent research shows that the internal activation of DNNs trained for image inference is very useful for capturing the perceptual loss corresponding to human visual perception [46], [47]. In our experiments, we adopt DPD [47] as a complementary metric of MSE and SSIM to capture the perceptual indistinguishability of recovered images. For this measure, the higher value indicates lower indistinguishability between recovered images and original images.
- *Reprint accuracy*. Reprint accuracy [43] is used to measure the model classification accuracy with recovered images. It can be used to determine how much privacy has been lost in recovered photos as compared to the originals.

1) Analysis of Privacy Protection under MNIST Dataset: We first test the effectiveness of our proposed Privacy Partitioning under the MNIST dataset. The MNIST dataset contains 60,000 handwritten digit images, 10,000 of which are test samples and the remaining are training samples. As our target model, we use a five-layer ReLU-based fully-connected feed-forward neural network with 900 hidden units. In the training phase, we deploy the first two layers to each data owner's device while leaving the remaining layers in the cloud. Concretely, we train the model as well as defenders (described below) for 600 epochs with the batch size of 32, where the learning rate of the model and defender are set as 0.0001 and 0.001, respectively. The dropout technique

[48] with the probability of 0.15 is also utilized to prevent over-fitting. In the inference phase, the attacker is able to access the outputs of local layers and tries to recovery input images, where we adopt MSE and SSIM as the distance metric (i.e., $d(\boldsymbol{x}, f_{\Theta_{d_i}}(f_{\Theta_l}(\boldsymbol{x})))$ shown in Eqn.(3)) to measure the indistinguishability between recovered images by attacks and original images.

To facilitate analysis, we set the weight μ used to embedding the fingerprint as 0.2, and the threshold τ is set to 0.85. The length of the fingerprint is set to 302 binary bits, which consists of a Community Relationship Code with a length of 60 bits and two independent Customer Identity Code with a length of 121 bits. This can accommodate a total of $N = \frac{121(120)}{11(10)} \times \frac{121(120)}{11(10)} = 17421$ customers and resist up to $k = 11 - 1 = 10$ colluders. Such parameter settings are sufficient for real scenarios and are also used in subsequent experiments for fingerprint performance estimation. Note that to evaluate the performance of privacy partitioning, the above parameter settings for embedding fingerprints are also used in the datasets LFW and CIFAR-10. To avoid redundancy, we will not repeat them.

TABLE I: Multiple attacks versus single defense under the MNIST dataset

	MSE	SSIM	Model Accuracy(%)
$\texttt{Attack}_1$	0.081	0.498	96.85
$\texttt{Attack}_2$	0.082	0.497	96.85
$\texttt{Attack}_3$	0.023	0.805	96.85
$\texttt{Attack}_4$	0.024	0.756	96.85
$\texttt{Attack}_5$	0.073	0.535	96.85
$\texttt{Attack}_6$	0.089	0.453	96.85
$\texttt{Attack}_7$	0.074	0.511	96.85
$\texttt{Attack}_8$	0.048	0.661	96.85

Multiple Attacks Versus Single Defender: As described before, each data owner can independently construct a local defender during the training phase. To demonstrate the advantages of this way, we first assume that the local defender of each data owner is unified. Without loss of generality, we set the defender as a two-layer ReLU-based neural network. Attackers (e.g., the server) can access the outputs of each local network (i.e., hidden state $\mathcal{H}'$), and use them to construct architectures to recover input images. To test the ability to resist attacks under different architectures, the attacker network is constructed as a combination of different hyperparameters, such as the number of hidden layers, the type of activation function, and the number of neurons in each layer. In total, we select 8 different attack models as follows.

- $\texttt{Attack}_1$. $900 \rightarrow \texttt{Tanh} \rightarrow 900 \rightarrow \texttt{ReLU} \rightarrow 900 \rightarrow \texttt{Sigmoid}$
- $\texttt{Attack}_2$. $900 \rightarrow \texttt{ReLU} \rightarrow \texttt{dropout}(0.15) \rightarrow 900 \rightarrow \texttt{Sigmoid}$
- $\texttt{Attack}_3$. $900 \rightarrow \texttt{Tanh} \rightarrow 900 \rightarrow \texttt{Sigmoid}$
- $\texttt{Attack}_4$. $900 \rightarrow \texttt{Tanh} \rightarrow 900 \rightarrow \texttt{Sigmoid} \rightarrow 900 \rightarrow \texttt{Sigmoid}$
- $\texttt{Attack}_5$. $600 \rightarrow \texttt{ReLU} \rightarrow 600 \rightarrow \texttt{Sigmoid}$
- $\texttt{Attack}_6$. $1024 \rightarrow \texttt{ReLU} \rightarrow 1024 \rightarrow \texttt{Sigmoid}$
- $\texttt{Attack}_7$. $1 - \texttt{Dconv} \rightarrow \texttt{Tanh} \rightarrow 900 \rightarrow \texttt{Sigmoid}$
- $\texttt{Attack}_8$. $900 \rightarrow \texttt{Sigmoid}$

We record the model accuracy and the quality of recovered images (denoted as MSE and SSIM). Table 1 displays the results. We can see that as the weight of the defender increases for each attack model, the overall trend of MSE increases (SSIM decreases), but the model's accuracy remains high ($> 96\%$). This demonstrates that adding defenders (with 304-bit fixed-length fingerprint) during training makes it harder for attackers to recover input images while maintaining a high model accuracy. We can see that the images recovered by the attacker are difficult to identify in the presence of a defender. However, it is insufficient to set a unified defender for every data owner. For example, for some attack models, such as $\texttt{attack}_3$ and $\texttt{attack}_4$, we can find that the MSE is still small (SSIM is still high) compared to other rows[5], which means that a single defender cannot resist various types of attacks. In the following subsection, we extend the single defender to multiple defenders and then demonstrate the advantages of this change.

TABLE II: Multiple attacks versus multiple defenders under the MNIST dataset

Defender Setting		No defender	Single defender	Multiple defenders
Model Accuracy		97.67	96.85	95.71
$MSE/SSIM$	$\texttt{Attack}_1$	0.068/0.542	0.081/0.498	0.214/0.075
	$\texttt{Attack}_2$	0.074/0.522	0.082/0.497	0.210/0.097
	$\texttt{Attack}_3$	0.018/0.832	0.023/0.805	0.070/0.499
	$\texttt{Attack}_4$	0.024/0.781	0.024/0.756	0.072/0.493
	$\texttt{Attack}_5$	0.068/0.550	0.073/0.535	0.192/0.193
	$\texttt{Attack}_6$	0.076/0.512	0.089/0.453	0.201/0.116
	$\texttt{Attack}_7$	0.072/0.517	0.074/0.511	0.167/0.203
	$\texttt{Attack}_8$	0.033/0.731	0.048/0.661	0.190/0.158

Multiple Attacks Versus Multiple Defender: We have shown that it is difficult for a single defender to defend against various types of attacks in previous experiments. We mitigate this problem by requiring each data owner to independently select a custom defender. To facilitate the experiment, we choose four different defenders and randomly assign them to 20 data owners. The attack model is consistent with previous experiments, and we also choose MSE and SSIM as metrics. The detailed description of the selected defenders is as follows.

- $\texttt{Defender}_1$. $900 \rightarrow \texttt{Tanh} \rightarrow 900 \rightarrow \texttt{Sigmoid}$
- $\texttt{Defender}_2$. $900 \rightarrow \texttt{Sigmoid}$
- $\texttt{Defender}_3$. $900 \rightarrow \texttt{Tanh} \rightarrow 900 \rightarrow \texttt{Sigmoid}$
- $\texttt{Defender}_4$. $900 \rightarrow \texttt{Sigmoid} \rightarrow 900 \rightarrow \texttt{Sigmoid}$

As shown in Table 2, we can observe that the performance of each attack model is significantly degraded when multiple defenders are added to the training process, compared to the performance when there is a single or no defender. This is primarily due to the fact that training multiple defenders increases the randomness of the input image confusion, making it more difficult for the adversary to recover the input images.

2) Analysis of Privacy Protection under LFW and CIFAR-10 Dataset: We should choose the appropriate intermediate layer as the partition point to achieve an elegant balance of model utility and privacy.As a result, the adversary struggles to recover the input images while maintaining high model accuracy. To achieve this, we conduct experiments on the LFW and CIFAR-10 datasets, respectively, where LFW contains

[5]Generally speaking, the similarity between two pictures is considered low when MSE is greater than 0.05 and SSIM is less than 0.6.

13233 images of faces collected from the web. CIFAR-10 contains 60,000 images, of which 10,000 are test images and the others are training images. It is a benchmark dataset for object recognition. For the constructed training model, we select different partition points (denoted as $\texttt{pool}_1$, $\texttt{pool}_2$ and $\texttt{pool}_3$) and analyze their utility. The details of the training model, partition points, defenders and attack models, are shown as follows.

1) The DNNs model used in LFW dataset is shown as follows:

$\texttt{conv2d}\ \ 8 \times 8 \rightarrow \texttt{conv2d}\ \ 8 \times 8 \rightarrow \texttt{maxpool}\ \ (pool_1)\ \ 4 \times 4 \rightarrow \texttt{conv2d}\ \ 5 \times 5 \rightarrow \texttt{conv2d}\ \ 5 \times 5 \rightarrow \texttt{maxpool}\ \ (pool_2)\ \ 3 \times 3 \rightarrow \texttt{conv2d}\ \ 5 \times 5 \rightarrow \texttt{conv2d}\ \ 5 \times 5 \rightarrow \texttt{maxpool}\ \ (pool_3)\ \ 3 \times 3 \rightarrow \texttt{conv2d}\ \ 5 \times 5 \rightarrow \texttt{conv2d}\ \ 5 \times 5 \rightarrow \texttt{maxpool}\ \ 3 \times 3 \rightarrow 800 \rightarrow \texttt{dropout}(0.8) \rightarrow 800.$

Please keep in mind that each convolutional layer is followed by layers of ReLU activation and batch normalization.

2) The outputs of the first three pooling layers, namely $\texttt{pool}_1$, $\texttt{pool}_2$, and $\texttt{pool}_3$, were chosen as the partition point in our studies, since the outputs of these layers can be used to denote the different levels of abstraction of features extraction from the model. The defender is built based on the layer that was chosen for partition. For example, if the partition point is $\texttt{pool}_2$, the defender will be the reversed form of local layers, as seen below.

$\texttt{deconv2d}\ \ 5 \times 5 \rightarrow \texttt{deconv2d}\ \ 5 \times 5 \rightarrow \texttt{ReLU} \rightarrow \texttt{conv2d}\ \ 8 \times 8 \rightarrow \texttt{deconv2d}\ \ 8 \times 8 \rightarrow \texttt{tanh}.$

3) The attack models used in LFW dataset are also constructed based on which layer selected for partition, since the dimension of input layer may be different with different partition point. For example, if we select the $\texttt{pool}_2$ as the partition point, the attacks are shown as follows:

- $\texttt{Attack}_1$. $\texttt{deconv2d}\ \ 5 \times 5 \rightarrow \texttt{deconv2d}\ \ 5 \times 5 \rightarrow \texttt{ReLU} \rightarrow \texttt{conv2d}\ \ 8 \times 8 \rightarrow \texttt{deconv2d}\ \ 8 \times 8 \rightarrow \texttt{tanh}.$
- $\texttt{Attack}_2$. $4090 \rightarrow \texttt{ReLU} \rightarrow\rightarrow 12288 \rightarrow \texttt{Sigmoid}$
- $\texttt{Attack}_3$. $4090 \rightarrow \texttt{Tanh} \rightarrow \texttt{dropout}(0.15) \rightarrow 12288 \rightarrow \texttt{Sigmoid}$

4) In our CIFAR-10 experiment, we use the VGG-19 with batch-normalization as the training model. Defender's design is likewise comparable to that of prior experiments. For example, if the partition point is set at $\texttt{pool}_2$, the defender appears as follows:

$\texttt{deconv2d}\ \ 3 \times 3 \rightarrow \texttt{BatchNorm} \rightarrow \texttt{ReLU} \rightarrow \texttt{deconv2d}\ \ 3 \times 3 \rightarrow \texttt{BatchNorm} \rightarrow \texttt{ReLU} \rightarrow \texttt{deconv2d}\ \ 3 \times 3 \rightarrow \texttt{BatchNorm}.$

5) The attacks CIFAR-10 dataset are shown as follows:

- $\texttt{Attack}_1$. $\texttt{deconv2d}\ \ 3 \times 3 \rightarrow \texttt{BatchNorm} \rightarrow \texttt{ReLU} \rightarrow \texttt{deconv2d}\ \ 3 \times 3 \rightarrow \texttt{BatchNorm} \rightarrow \texttt{tanh} \rightarrow \texttt{deconv2d}\ \ 3 \times 3 \rightarrow \texttt{BatchNorm}.$
- $\texttt{Attack}_2$. $1024 \rightarrow \texttt{ReLU} \rightarrow\rightarrow 3072$
- $\texttt{Attack}_3$. $1024 \rightarrow \texttt{ReLU} \rightarrow \texttt{dropout}(0.15) \rightarrow 3027$

Similar to previous experiments, SSIM, MSE, DPD, and reprint accuracy are used to measure the difference between the input image and the restored image. We test the effectiveness of different attack models with defenders and record the results under the best attacks (shown in Fig. 4). Fig. 4(a) shows that our model still maintains a good classification accuracy ($> 88\%$) on both LFW and CIFAR-10 dataset. We notice that placing the partition point on a "deeper" layer results in a slight weakening of accuracy compared to placing it on a shallow layer. In fact, putting the partition point in a shallower layer is beneficial to the subsequent layers to offset the noise caused by the introduction of the defender, thereby helping to improve the accuracy of the model. Fig. 4(b) shows that placing the partition point in three different locations makes it difficult for the adversary to recover the input image. However, the reprint accuracy gradually decreases as we deploy the partition point in the deeper layers. This is well understood. As mentioned above, when the partition point is placed in a deeper layer, the noise caused by the defender will be relatively difficult to be fully offset. This will hurt the accuracy of the model to some extent, while increasing the difficulty of recovering the input image. In Fig. 4(c-e), it is obvious that privacy partitioning deteriorates the quality of the recovered image for all the metrics considered. In addition, the results also suggest that the partition point should be placed in deeper layers to achieve a better level of privacy protection. Appendix 1.5 give the results of the visualization.

Overall, it will be more secure if the partition point is placed in deeper layers. However, as mentioned earlier, this may compromise the classification accuracy of the model to some extent. In addition, deploying more layers locally will also compromise the intellectual property of DNNs. Therefore, in practical applications, the server needs to comprehensively consider various factors to make a trade-off between model utility and privacy.

B. Performance of Fingerprint

The above experiments have demonstrated the efficiency of Privacy Partitioning, and shown that the model still gives satisfactory classification accuracy under the fingerprint embedded with long bits (304 bits). The performance of the proposed fingerprint is discussed in this section. Because each customer's fingerprint is made up of the community relationship code and the customer identity code, as previously demonstrated, we first discuss the nature of the community relationship code while maintaining the neighborhood structure, and then demonstrate the robustness of the customer identity code against various attacks. Due to page constraints, we are only displaying the experimental results for the MNIST and CIFAR-10 datasets. The community relationship between users is simulated by three public social network datasets (shown below). Besides, all the parameters related to the Privacy Partitioning, such as the choice of defenders and attack models, are consistent with previous experiments.[6]

1) Analysis of CRC: In our SECUREMARK-DL, to represent the social network structure of customers, we employ community relationship code. Customers from similar communities will be assigned similar CRCs, but customers from unrelated areas will be assigned extremely different CRCs. This property allows the server to immediately identify

[6]Note that in the CIFAR-10 dataset, we only use $\texttt{pool}_2$ as the partition point for simplicity.

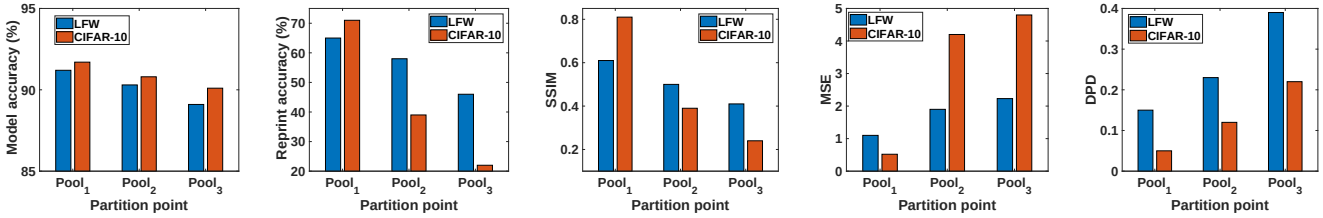

(a) (b) (c) (d) (e)

Fig. 4: Performance analysis with LFW and CIFAR-10. (a) Model accuracy. (b) Reprint accuracy. (c) SSIM. (d) MSE. (e) DPD

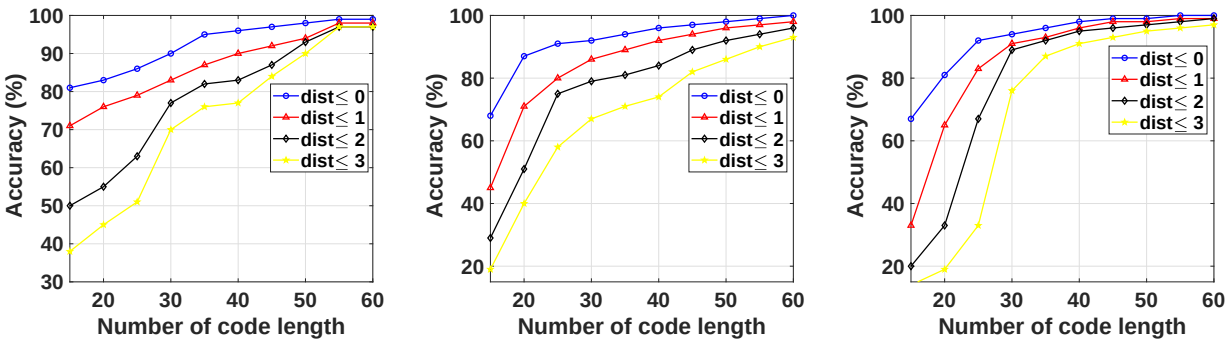

(a) (b) (c)

Fig. 5: The accuracy of CRC with different social networks. (a) Facebook. (b) Twitter. (c) Google

questionable consumer groups. To demonstrate this, we use the Stanford Network Analysis Platform (SNAP) [7] to obtain three public social network datasets and run experimental simulations on them. Each dataset is a large-scale adjacency graph, with each node representing a customer in our study and the edge between two points representing the link between the two entities. The following is a list of each dataset's comprehensive information.

- `Facebook` is an undirected graph of 88234 edges and 4039 nodes, with each node (i.e., customer) divided into ten communities.
- `Twitter` is a directed graph with 1,768,149 edges and 81,306 customers, and all customers are classified into 1,000 communities.
- `Google` is a directed graph with 13673453 edges and 107614 customers. and all customers are classified into 133 communities.

We select CRCs with different lengths (ranging from 15 to 60 bits) and evaluated their performance on three datasets. The results are shown in Fig. 5, where p_{ij} is used to represent the Hamming distance between the community relationship code of customer i and j. In the implementation process, if p_{ij} is less than the given threshold distance $dist \in [0, 3]$, then $p_{ij} = 1$, otherwise $p_{ij} = 0$. We can obtain the accuracy of preserving the neighborhood structure of CRC under different social networks in this manner. The CRCs, as shown in Fig. 5, can accurately preserve the neighborhood structure between different customers. Furthermore, as the length of the code increases, so does the trend of accuracy.

2) Analysis of CIC: As previously stated, BIBD is used to generate a unique CIC for each customer. Such CICs ensure that the synthesized code of any K or fewer customer identity codes remains unique. Besides, the inexplicability of the model makes the embedded fingerprints integrated as a component of the parameters, so that the adversary cannot accurately locate where the fingerprint is embedded in the model. This makes our designed fingerprint robust to various attacks. To demonstrate this, we adopt two separate $(121, 11, 1)$-BIBD AND-ACC codebooks to generate the CIC. It can accommodate a total of $N = \frac{121(120)}{11(10)} \times \frac{121(120)}{11(10)} = 17421$ customers and resist up to $k = 11 - 1 = 10$ colluders. We use the MNIST and CIFAR-10 datasets for fingerprint embedding respectively. The threshold τ used in extraction is set to 0.85, and the weight μ of the embedded fingerprint is set to 0.2.

Collusion Attack: We focus on the average fingerprint collusion attack, which is a traditional and cost-effective attack method. The principle of the attack has been described in Section IV. We record the detection rate of (121,11,1)-BIBD CIC with different numbers of colluders, as shown in Fig. 6(a). It is clear that when the number of conspirators is 10 or less, the detection rate remains at 100%, which is consistent with the nature of the (121,11,1)-BIBD CIC. On both datasets, we

[7] http://snap.stanford.edu/

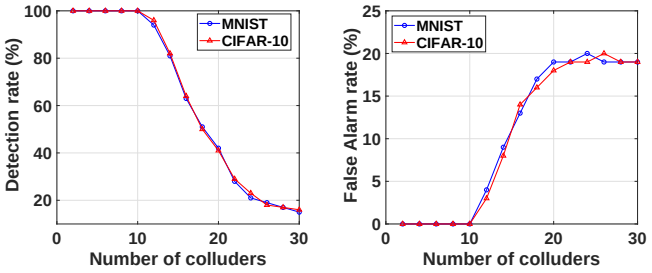

(a) (b)

Fig. 6: The performance of $(121, 11, 1)$-BIBD CIC with collusions. (a) Detection rate. (b) False alarm rate.

also track the false alarm rate. Fig. 6(b) depicts the results. When the number of colluders does not exceed 10, the error rate remains constant at 0%, which is also consistent with the previous maximum detectable number $k = 10$.

To study the difference between CICs with different lengths, we conduct experiments to compare the effectiveness of $(121, 11, 1)$-BIBD code and $(49, 7, 1)$-BIBD code on collusion attacks, where the $(49, 7, 1)$-BIBD has a collusion resilience level $k = 7 - 1 = 6$. As shown in Fig. 7, we can observe that $(121, 11, 1)$-BIBD code has a better detection rate as well as false alarm rate than $(49, 7, 1)$-BIBD code. However, compared with $(49, 7, 1)$-BIBD code, $(121, 11, 1)$-BIBD code is required to allocate more bits for each customer, which may hurt the model accuracy when more bits are embedded in the model. Therefore, in practical applications, the server needs to make a trade-off based its desired collusion resilience requirement.

Model Fine-tuning Attack: Next we discuss the performance of the fingerprint we designed under the model fine-tuning attack. Specifically, given the original optimization function (shown in Eqn.(1)), we retrained the fingerprinted model with the model Fine-tuning attack proposed in [49], which is widely recognized as one of the most advanced attack methods. We allow the attacker to have access to a benign dataset of the same size as the data owner, and can perform retraining at 10% of the total batches required for the original training.[8] The results are described in Fig. 8(a) and Fig. 8(b). It can be seen that when the number of conspirators does not exceed 10, the detection rate remains at 100%, and the error rate always remains at 0%. This is also consistent with the results shown in the previous experiment (refer to Fig. 6). Hence, our CIC can resist model fine-tuning attacks.

Model Compression Attack: Finally, we discuss the effectiveness of CIC against model compression attacks. We consider parameter pruning, a very common model compression method. Specifically, we exploit the strategy designed in [50] to prune the target layer, that is, setting the $\alpha\%$ of the weight with the smallest weight values to zero. On top of this, to compensate for the accuracy drop caused by pruning, the fingerprinted model is sparsely fine-tuned with the cross-entropy loss on the original training set. We record the collusion-detection accuracy of customer identity code under parameter pruning with different rates ($\alpha\%$). The results for the MNIST and CIFAR-10 datasets are shown in Fig. 9. The detection accuracy and false alarm rate both increase as the proportion of trimming parameters increases. When the number of conspirators is less than 10, however, the detection rate is 100 percent, and the error rate is always zero percent. As a result, the model compression attack is effectively mitigated by our CIC.

[8]Obviously, if the adversary has unlimited computing resources to retrain the target model, the fingerprint embedded in the model can eventually be removed. However, this is illogical because an adversary with powerful computing and data resources can build another functionally-equivalent model of its own. Therefore, we assume here that the adversary has limited resources, and its maximum capability is limited to only 10% of the total batches required to train the original model for model fine-tuning. This is also the assumption followed by most model fine-tuning attacks.

TABLE III: Comparison of computation overhead

Dataset	FP Embedding	FP Extraction
MNIST	5.424%	0.007%
CIFAR-10	2.413%	0.059%

3) Analysis of the Efficiency of Fingerprint Embedding and Extraction: Since the fingerprint (FP) for each user is embedded by training the model using an additional regularization term, which means the model has to be re-trained every time to embed a unique fingerprint for each customer. To demonstrate the negligible computational overhead incurred in this process, we separately record the ratio of the overhead for embedding and extracting fingerprints to the total cost of training the model under the MNIST and CIFAR-10 datasets. The results are summarized in Table 3, where we can see that compared with the overhead required for training the model, the running time required for fingerprint embedding and extraction is almost negligible. This also confirms the practicality of SECUREMARK-DL.

VII. RELATED WORK

A. Privacy-preserving Deep Learning

In summary, existing privacy-preserving distributed deep learning approaches are mostly evolved from two underlying techniques: *Cryptographic primitive-based technologies* [8], [9] and *Differential Privacy* [11], [12]. Commonly used cryptographic techniques include Secure Multiparty Computing (SMC) and homomorphic encryption. For example, *Aono et al.* [9] designed a secure distributed deep learning framework. The authors resorted to the LWE-based homomorphic encryption to encrypt the local gradients shared with the multiple participants. Moreover, in the training process, asynchronous stochastic gradient descent and secure channels are used to improve the efficiency and security of communication. *Bonawitz et al.* [26] also designed a secure federated training structure. With the diffie-hellman key exchange protocol and shmair secret sharing strategy, the proposed model can ensure that users share parameters privately even if there are abnormal situations, such as users dropping out, network interruption, and equipment damage. However, *Cryptographic primitive-based technologies* inevitably incur huge computational or

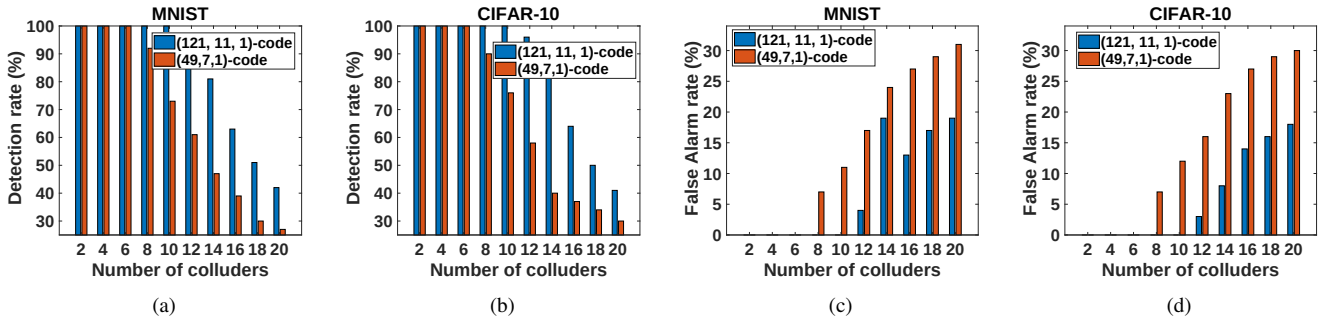

Fig. 7: Performance comparison between $(121, 11, 1)$-BIBD CIC and $(49, 7, 1)$-BIBD CIC. (a) Detection rate under MNIST dataset. (b) Detection rate under CIFAR-10 dataset. (c) False alarm rate under MNIST dataset. (d) False alarm rate under CIFAR-10 dataset.

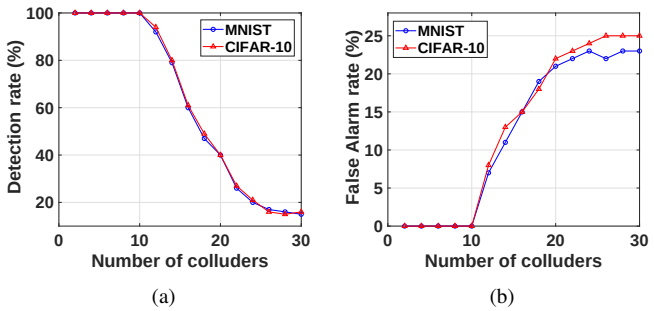

Fig. 8: The performance of $(121, 11, 1)$-BIBD CIC with model fine-tuning. (a) Detection rate. (b) False alarm rate.

communication burdens, as well as not suitable for distributed training scenarios, where data providers are typically mobile devices with limited computing capabilities and storage.

Compared with cryptography-based protocols, privacy-preserving deep leaning with differential privacy [11], [12] is outstanding in performance. It only requires data owners to perturb sensitive data before sharing them, and ensures the data perturbation mechanism satisfies a pre-set privacy budget. Unfortunately, the state-of-the-art result [13] has shown that current deep learning mechanisms based on differential privacy rarely provide acceptable utility-privacy trade-offs for complex learning tasks. Moreover, recent research [14] has verified that distributed, federated, or decentralized deep learning approach is fundamentally broken even all parameters are obfuscated via differential privacy. Recently, the technology of privacy partitioning was proposed [30] to alleviate the above problems. Privacy partitioning is to split the training model, and adds the penalty function into the optimization function to realize the privacy protection of the training data. Unfortunately, the original privacy partition does not perfectly support distributed deep learning. It requires a trusted third party to collect user data and interact with the server, which is inconsistent with most applications in real life.

B. Watermarking for Deep Learning

Watermarking technologies are widely used in DNNs to provide verification channels for the intellectual property of the model. For example, *Adi et al.* [15] designed to use backdoors to embed watermarks. *Rouhani et al.* [16] presented DeepSigns, which embeds a given secret into the probability density function of the DNN model. *Namba et al.* [51] exploit the method of exponential weighting to guide the watermarking process, i.e., it exponentially increases the weight that affects the prediction result significantly during the watermark embedding process. Other works, like [17]–[22], achieved similar goals using various technologies, including adversarial examples [17], [18], regularization parameter [19], [20] and backdoors based technologies [21], [22]. However, as presented before, existing work exclusively focuses on whether the target model is infringed with copyright, and rarely considers tracking of pirates. To the best of our knowledge, only *Chen et al.* [52] proposed the first end-to-end piracy tracking model. The authors also used balanced in-complete block design (BIBD) to generate fingerprints and prevented collusion attacks from multiple customers. However, their solution is not suitable for collusion detection in a large-scale customers environment, because the relationship between customers is not considered in the process of fingerprint design. Moreover, work [52] also neglected the privacy protection of the samples involved in the training process.

VIII. Conclusion

We propose SecureMark-DL, the first privacy-preserving deep learning framework with model ownership protection and traitor tracing. Extensive experiments on the MINIST LFW and CIFAR10 datasets and different types of DNNs, show that SecureMark-DL outperforms existing works in terms of training accuracy, privacy, and robustness. Future research in this area will concentrate on improving the security and efficiency of SecureMark-DL.

References

[1] J. Wang, L. Gou, W. Zhang, H. Yang, and H.-W. Shen, "Deepvid: Deep visual interpretation and diagnosis for image classifiers via knowledge distillation," *IEEE Transactions on Visualization and Computer Graphics*, vol. 25, no. 6, pp. 2168–2180, 2019.

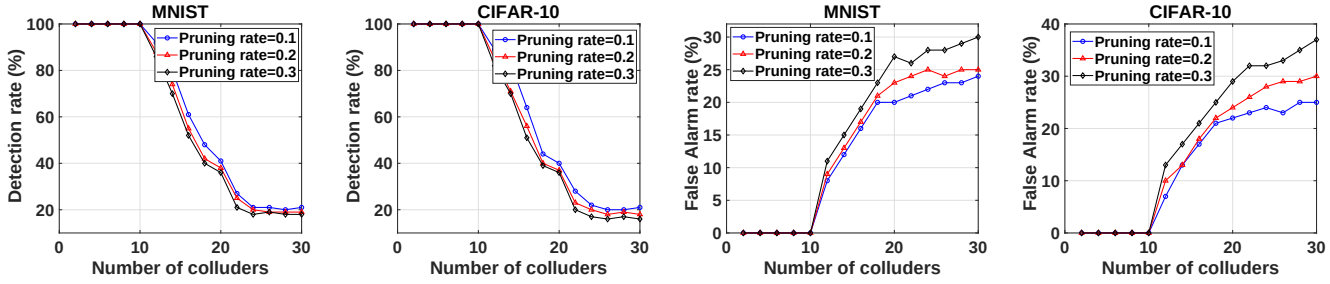

Fig. 9: The performance of $(121, 11, 1)$-BIBD CIC with parameter pruning. (a) Detection rate under MNIST. (b) Detection rate under CIFAR-10. (c) False alarm rate under MNIST. (d) False alarm rate under CIFAR-10.

[2] M. I. Georgescu, R. Ionescu, F. S. Khan, M. Popescu, and M. Shah, "A background-agnostic framework with adversarial training for abnormal event detection in video," *IEEE Transactions on Pattern Analysis and Machine Intelligence*, pp. 1–1, 2021.

[3] G. Xu, H. Li, Y. Zhang, X. Lin, R. H. Deng, and X. Shen, "A deep learning framework supporting model ownership protection and traitor tracing," in *Proceedings of the IEEE ICPADS*, 2020, pp. 1–9.

[4] "Amazon rekognition," https://aws.amazon.com/rekognition/.

[5] "Microsoft azure computer vision," https://azure.microsoft.com/en-us/services/cognitive-services/computer-vision/#overview.

[6] "Google cloud vision ai," https://cloud.google.com/vision.

[7] J. Zhang, D. Chen, J. Liao, W. Zhang, H. Feng, G. Hua, and N. Yu, "Deep model intellectual property protection via deep watermarking," *IEEE Transactions on Pattern Analysis and Machine Intelligence*, pp. 1–1, 2021.

[8] H. Wu, G. Liu, Y. Yao, and X. Zhang, "Watermarking neural networks with watermarked images," *IEEE Transactions on Circuits and Systems for Video Technology*, 2020.

[9] Y. Aono, T. Hayashi, L. Wang, S. Moriai *et al.*, "Privacy-preserving deep learning via additively homomorphic encryption," *IEEE Transactions on Information Forensics and Security*, vol. 13, no. 5, pp. 1333–1345, 2017.

[10] J. Xu, W. Zhang, and F. Wang, "$a(dp)^2$sgd: Asynchronous decentralized parallel stochastic gradient descent with differential privacy," *IEEE Transactions on Pattern Analysis and Machine Intelligence*, pp. 1–1, 2021.

[11] R. Shokri and V. Shmatikov, "Privacy-preserving deep learning," in *Proceedings of the ACM CCS*, 2015, pp. 1310–1321.

[12] M. Abadi, A. Chu, I. Goodfellow, H. B. McMahan, I. Mironov, K. Talwar, and L. Zhang, "Deep learning with differential privacy," in *Proceedings of the ACM CCS*, 2016, pp. 308–318.

[13] B. Jayaraman and D. Evans, "Evaluating differentially private machine learning in practice," in *Proceedings of the USENIX Security*, 2019, pp. 1–18.

[14] B. Hitaj, G. Ateniese, and F. Perez-Cruz, "Deep models under the gan: information leakage from collaborative deep learning," in *Proceedings of the ACM CCS*, 2017, pp. 603–618.

[15] Y. Adi, C. Baum, M. Cisse, B. Pinkas, and J. Keshet, "Turning your weakness into a strength: Watermarking deep neural networks by backdooring," in *Proceedings of USENIX Security*, 2018, pp. 1615–1631.

[16] B. Darvish Rouhani, H. Chen, and F. Koushanfar, "Deepsigns: An end-to-end watermarking framework for ownership protection of deep neural networks," in *Proceedings of ACM ASPLOS*, 2019, pp. 485–497.

[17] E. L. Merrer, P. Perez, and G. Trédan, "Adversarial frontier stitching for remote neural network watermarking," *arXiv preprint arXiv:1711.01894*, 2017.

[18] S. Szyller, B. G. Atli, S. Marchal, and N. Asokan, "Dawn: Dynamic adversarial watermarking of neural networks," *arXiv preprint arXiv:1906.00830*, 2019.

[19] Z. Yang, H. Dang, and E.-C. Chang, "Effectiveness of distillation attack and countermeasure on neural network watermarking," *arXiv preprint arXiv:1906.06046*, 2019.

[20] Y. Uchida, Y. Nagai, S. Sakazawa, and S. Satoh, "Embedding watermarks into deep neural networks," in *Proceedings of ACM ICMR*. ACM, 2017, pp. 269–277.

[21] J. Guo and M. Potkonjak, "Watermarking deep neural networks for embedded systems," in *Proceedings of IEEE/ACM ICCAD*. IEEE, 2018, pp. 1–8.

[22] J. Zhang, Z. Gu, J. Jang, H. Wu, M. P. Stoecklin, H. Huang, and I. Molloy, "Protecting intellectual property of deep neural networks with watermarking," in *Proceedings of ACM AsiaCCS*, 2018, pp. 159–172.

[23] M. Wu, W. Trappe, Z. J. Wang, and K. R. Liu, "Collusion-resistant fingerprinting for multimedia," *IEEE Signal Processing Magazine*, vol. 21, no. 2, pp. 15–27, 2004.

[24] H. V. Zhao, M. Wu, Z. J. Wang, and K. R. Liu, "Forensic analysis of nonlinear collusion attacks for multimedia fingerprinting," *IEEE Transactions on Image Processing*, vol. 14, no. 5, pp. 646–661, 2005.

[25] D. Boneh and J. Shaw, "Collusion-secure fingerprinting for digital data," in *Proceedings of Cryptology*. Springer, 1995, pp. 452–465.

[26] K. Bonawitz, V. Ivanov, B. Kreuter, A. Marcedone, H. B. McMahan, S. Patel, D. Ramage, A. Segal, and K. Seth, "Practical secure aggregation for privacy-preserving machine learning," in *Proceedings of the ACM CCS*, 2017, pp. 1175–1191.

[27] P. Mohassel and Y. Zhang, "Secureml: A system for scalable privacy-preserving machine learning," in *Proceedings of the IEEE Security and Privacy*, 2017, pp. 19–38.

[28] C. Liu, H. Ling, F. Zou, and L. Yan, "Neighborhood preserving hashing for fast similarity search," in *Proceedings of the 20th ACM international conference on Multimedia*. ACM, 2012, pp. 945–948.

[29] L. A. Bassalygo and V. A. Zinoviev, "Remark on balanced incomplete block designs, near-resolvable block designs, and q-ary constant-weight codes," *Problems of Information Transmission*, vol. 53, no. 1, pp. 51–54, 2017.

[30] J. Chi, E. Owusu, X. Yin, T. Yu, W. Chan, P. Tague, and Y. Tian, "Privacy partitioning: Protecting user data during the deep learning inference phase," *arXiv preprint arXiv:1812.02863*, 2018.

[31] C. L. Apicella, F. W. Marlowe, J. H. Fowler, and N. A. Christakis, "Social networks and cooperation in hunter-gatherers," *Nature*, vol. 481, no. 7382, p. 497, 2012.

[32] Y. Yu, Z. Wei, X. Chen, and Z. Zhang, "Group-oriented and collusion secure fingerprint for digital images," *Journal of Computers*, vol. 6, no. 2, pp. 200–207, 2011.

[33] B.-Y. Sun, X.-M. Zhang, J. Li, and X.-M. Mao, "Feature fusion using locally linear embedding for classification," *IEEE transactions on neural networks*, vol. 21, no. 1, pp. 163–168, 2009.

[34] D. D. Lee and H. S. Seung, "Algorithms for non-negative matrix factorization," in *Advances in neural information processing systems*, 2001, pp. 556–562.

[35] F. Sha, L. K. Saul, and D. D. Lee, "Multiplicative updates for nonnegative quadratic programming in support vector machines," in *Advances in neural information processing systems*, 2003, pp. 1065–1072.

[36] C.-J. Lin, "On the convergence of multiplicative update algorithms for nonnegative matrix factorization," *IEEE Transactions on Neural Networks*, vol. 18, no. 6, pp. 1589–1596, 2007.

[37] ——, "Projected gradient methods for nonnegative matrix factorization," *Neural computation*, vol. 19, no. 10, pp. 2756–2779, 2007.

[38] B. Schölkopf, "The kernel trick for distances," in *Advances in neural information processing systems*, 2001, pp. 301–307.

[39] M. Marchetti and D. Stabili, "Read: Reverse engineering of automotive

data frames," *IEEE Transactions on Information Forensics and Security*, vol. 14, no. 4, pp. 1083–1097, 2019.
[40] S. He and M. Wu, "Collusion-resistant video fingerprinting for large user group," *IEEE Transactions on Information Forensics and Security*, vol. 2, no. 4, pp. 697–709, 2007.
[41] ——, "Joint coding and embedding techniques for multimediafingerprinting," *IEEE Transactions on Information Forensics and Security*, vol. 1, no. 2, pp. 231–247, 2006.
[42] W. Sun, B. Zheng, and W. Qian, "Computer aided lung cancer diagnosis with deep learning algorithms," in *Medical imaging 2016: computer-aided diagnosis*, vol. 9785. International Society for Optics and Photonics, 2016, p. 97850Z.
[43] M. Mathieu, C. Couprie, and Y. LeCun, "Deep multi-scale video prediction beyond mean square error," *arXiv preprint arXiv:1511.05440*, 2015.
[44] J. Kim and S. Lee, "Deep learning of human visual sensitivity in image quality assessment framework," in *Proceedings of the IEEE conference on computer vision and pattern recognition*, 2017, pp. 1676–1684.
[45] Z. Yin and J. Shi, "Geonet: Unsupervised learning of dense depth, optical flow and camera pose," in *Proceedings of the IEEE Conference on Computer Vision and Pattern Recognition*, 2018, pp. 1983–1992.
[46] R. Zhang, P. Isola, A. A. Efros, E. Shechtman, and O. Wang, "The unreasonable effectiveness of deep features as a perceptual metric," in *Proceedings of the IEEE Conference on Computer Vision and Pattern Recognition*, 2018, pp. 586–595.
[47] A. Dosovitskiy and T. Brox, "Generating images with perceptual similarity metrics based on deep networks," in *Advances in neural information processing systems*, 2016, pp. 658–666.
[48] X. Zhang, X. Zhou, M. Lin, and J. Sun, "Shufflenet: An extremely efficient convolutional neural network for mobile devices," in *Proceedings of IEEE CVPR*, 2018, pp. 6848–6856.
[49] X. Chen, W. Wang, C. Bender, Y. Ding, R. Jia, B. Li, and D. Song, "Refit: a unified watermark removal framework for deep learning systems with limited data," *arXiv preprint arXiv:1911.07205*, 2019.
[50] S. Han, J. Pool, J. Tran, and W. J. Dally, "Learning both weights and connections for efficient neural networks," in *Proceedings of the 28th International Conference on Neural Information Processing Systems*, 2015, pp. 1135–1143.
[51] R. Namba and J. Sakuma, "Robust watermarking of neural network with exponential weighting," *arXiv preprint arXiv:1901.06151*, 2019.
[52] H. Chen, B. D. Rouhani, C. Fu, J. Zhao, and F. Koushanfar, "Deepmarks: A secure fingerprinting framework for digital rights management of deep learning models," in *Proceedings of the 2019 on International Conference on Multimedia Retrieval*. ACM, 2019, pp. 105–113.